Short communication

Novel iron oxide nanotube arrays as high-performance anodes for lithium ion batteries

CrossMark

Yuan Zhong [a], Huiqing Fan [a], Ling Chang [a], Haibo Shao [a, b], Jianming Wang [a, *], Jianqing Zhang [a, b], Chu-nan Cao [a, b]

[a] Department of Chemistry, Zhejiang University, Hangzhou 310027, PR China
[b] Institute of Electrochemistry and Functional Materials, Zhejiang University, Hangzhou 310027, PR China

HIGHLIGHTS

- Iron oxalate nanotube arrays are fabricated by a novel self-corrosion method.
- Iron oxide/carbon composite nanotube arrays are achieved by the annealing treatment.
- The composite nanotube arrays show high electrochemical cycling stability.
- The composite nanotube arrays exhibit prominent rate capability.

GRAPHICAL ABSTRACT
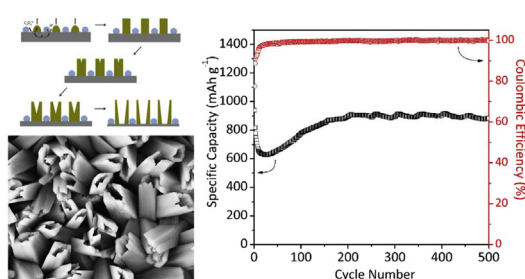
ARTICLE INFO

ABSTRACT

Nanostructured iron oxides can be promising anode materials for lithium ion batteries (LIBs). However, improvement on the rate capability and/or electrochemical cycling stability of iron oxide anode materials remains a key challenge because of their poor electrical conductivities and large volume expansion during cycling. Herein, the vertically aligned arrays of one-dimensional (1D) iron oxide nanotubes with 5.8 wt% carbon have been fabricated by a novel surfactant-free self-corrosion process and subsequent thermal treatment. The as-fabricated nanotube array electrode delivers a reversible capacity of 932 mAh g^{-1} after 50 charge–discharge cycles at a current of 0.6 A g^{-1}. The electrode still shows a reversible capacity of 610 mAh g^{-1} even at a very high rate (8.0 A g^{-1}), demonstrating its prominent rate capability. Furthermore, the nanotube array electrode also exhibits the excellent electrochemical cycling stability with a reversible capacity of 880 mAh g^{-1} after 500 cycles at a current of 4 A g^{-1}. The nanotube array electrode with superior lithium storage performance reveals the promising potential as a high-performance anode for LIBs.

© 2015 Elsevier B.V. All rights reserved.

1. Introduction

As one of the critical electrochemical energy storage devices, lithium ion batteries (LIBs) have drawn world-wide interest for their extensive applications, including portable electronics, electric vehicle, and stationary storage for intermittent energy sources [1,2]. With the ever-increasing demand for high-performance LIBs, the low capacity (<372 mAh g^{-1}) of commercial graphite anode has become a limiting factor for practical applications [1]. Intensive investigations on alternative anode materials have been conducted. Metal oxides such as Fe$_2$O$_3$ [3–6], Fe$_3$O$_4$ [7–10], Co$_3$O$_4$ [11–13], NiO [14,15] and SnO$_2$ [16–18] are attractive due to their large lithium

storage capacities. Among the investigated metals oxides, iron oxides are considered as promising anode materials for LIBs owing to their high theoretical capacities, low cost, environmentally benign nature and improved safety [19,20]. However, because of the low electrical conductivities and large volume expansion during cycling, iron oxides as anode materials generally show poor rate capability and/or low electrochemical cycling stability, significantly limiting their practical applications in LIBs. During the past decades, various strategies have been probed to improve the lithium storage properties of iron oxides. One effective strategy is the rational design and synthesis of diverse iron oxide nanomaterials. Various iron oxide nanostructures have been reported as anode materials for LIBs, including nanoparticles [10,21], nanowires [22,23], nanotubes [24–26], nanosheets [6,27,28] and other nanostructures [29–31]. These nanostructured iron oxide anodes for LIBs show improved electrochemical performance. Another commonly used approach is to use the hybrid nanostructures of iron oxides and carbon materials (including amorphous carbon, carbon nanotubes and graphene) [20,21,31]. The introduced carbon materials may improve the electrical conductivities of iron oxides, thus enhancing their lithium storage performance. Despite the progress mentioned above, the rate capability and cycling stability of iron oxides as anode materials for LIBs need to be further enhanced. The rational design and controllable synthesis of high-performance iron oxide anode materials for LIBs remain a great challenge.

In this work, we fabricate the vertically aligned arrays of 1D iron oxide nanotubes with 5.8 wt% carbon by a novel surfactant-free self-corrosion process and subsequent thermal treatment, as illustrated in Fig. S1 (Supporting Information). The as-fabricated nanotube array electrodes show the superior lithium storage performance.

2. Experimental

An iron film was prepared by a cathodic electrodeposition in the electrolyte solution with 163 g L^{-1} FeSO$_4$·7H$_2$O and 100 g L^{-1} (NH$_4$)$_2$SO$_4$ at room temperature. The deposition process was conducted in a two-electrode cell with a platinum counter electrode. A copper foil with an exposed area of 1.8 cm^2 was assembled as the working electrode. Prior to deposition, the copper foil was polished with 2000# grit waterproof abrasive paper, and ultrasonically cleaned in acetone and deionized water for 10 min, respectively. The iron film was deposited at a constant current density of 6 mA cm^{-2}, and the deposition time was 3 min. After rinsed extensively with deionized water and dried in a nitrogen stream, the copper foil with the electrodeposited Fe film was immersed in 0.3 M oxalic acid ethanol solution with 50wt% H$_2$O at 60 °C for 1 h, unless otherwise noted. After washed by ethanol and dried in air, the obtained iron oxalate hydrate film was annealed at 300 °C for 2 h in a H$_2$-filled tube furnace to get the FeO$_x$/C film.

The X-ray diffraction (XRD) patterns of film electrodes were recorded using a Rigaku D/Max 2550 X-ray diffractometer with Cu Kα radiation at 40 kV and 300 mA. The morphology and microstructure of various films were observed by scanning electron microscopy (SEM) using a ZEISS, ULTRA™ 55 with an accelerating voltage of 5 kV and transmission electron microscopy (TEM) using a Philips-FEI Teanai G2 F30 with an accelerating voltage of 300 kV. Raman spectra were recorded using a Jobin Yvon Labor Raman series HR-800 with an excitation wavelength of 514 nm. The X-ray photoelectron spectroscopy (XPS) was recorded using VG ESCALAB MARK II with Mg Kα(1235.6 eV) radiation. The content of carbon was determined by organic element analysis method using an Elementar Vario MICRO Cube. The iron(II) amount in the immersion solution was analyzed by inductively coupled plasma atomic emission spectroscopy (ICP, SPECTRO) on a Thermo Electron

Corporation IRIS Intrepid II XSP instrument. The masses of various films were determined by a microbalance (Sartorius BT25S).

The formation reaction of FeC$_2$O$_4$·2H$_2$O was as follows:

$$Fe(s) + H_2C_2O_4(l) + 2H_2O(l) = H_2\uparrow + FeC_2O_4\cdot 2H_2O(s) \qquad (1)$$
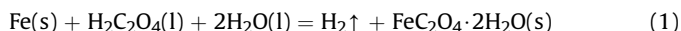
According to equation (1), the mass of FeC$_2$O$_4$·2H$_2$O on the substrate was calculated in terms of the iron(II) amount in the immersion solution and the masses of the substrate with the surface films before and after the immersion. The total mass of active materials (including Fe$_2$O$_3$, Fe$_3$O$_4$ and C) in the annealed film was determined according to the mass of FeC$_2$O$_4$·2H$_2$O and the mass loss induced by the annealing treatment in H$_2$ atmosphere.

The electrochemical measurements were carried out at room temperature (25 °C) using coin cells (CR2025) with lithium metal as the counter and reference electrodes. The as-prepared FeO$_x$/C film was directly used as the working electrode. The total mass of active materials (including Fe$_2$O$_3$, Fe$_3$O$_4$ and C) in the working electrode was determined to be 0.21 mg cm^{-2}. 1 M LiPF$_6$ in a 1:1 w/w mixture of ethylene carbonate (EC) and dimethyl carbonate (DMC) was used as the electrolyte, and a polypropylene membrane (Celgard 2325) was used as the separator. Cell assembly was conducted in an Ar-filled glovebox. Galvanostatic charge–discharge cycles of the cells were measured between 3.0 and 0.05 V at various rates with a LAND CT2001A battery testing system. Cyclic voltammetry (CV) measurements were carried out using a CHI630d electrochemical workstation at the scan rate of 0.1 mV s^{-1} between 0 and 3 V.

3. Results and discussion

The XRD patterns of as-prepared film electrode before and after the thermal treatment in H$_2$ atmosphere are illustrated in Fig. 1a and b. The XRD peaks in Fig. 1a can be ascribed to orthorhombic β-FeC$_2$O$_4$·2H$_2$O, Cu and Fe according to IDSC PDF 22−0635, 01−1421 and 01−1252, indicating that Fe is turned into β-FeC$_2$O$_4$·2H$_2$O by the immersion in the oxalic acid solution. It can be seen from Fig. 1b that the XRD peaks for β-FeC$_2$O$_4$·2H$_2$O disappear, and new XRD peaks occur. The peaks located at 2θ = 18.3°, 24.2°, 30.0°, 35.7°, 57.5° and 62.2° in Fig. 1b can be indexed as crystal planes (111) for Fe$_3$O$_4$, (012) for Fe$_2$O$_3$, (220) for Fe$_3$O$_4$, (110) for Fe$_2$O$_3$, (122) for Fe$_2$O$_3$ and (214) for Fe$_2$O$_3$ in terms of IDSC PDF 01−1111 and 01−1053, respectively. This shows that Fe$_2$O$_3$ and Fe$_3$O$_4$ phases are obtained by the thermal treatment. The Raman spectra of as-prepared film electrode before and after the thermal treatment are shown in Fig. 1c. The characteristic peak of C$_2$O$_4^{2-}$ located at 1480 cm^{-1} disappears after thermal treatment [32]. The Raman peaks at 216, 284, 402, 493 and 601 cm^{-1} are assigned to the A$_{1g}$ and E$_g$ modes of Fe$_2$O$_3$ [33]. The Raman peak at 670 cm^{-1} results from the A$_{1g}$ mode of Fe$_3$O$_4$ [34]. The peak at 1590 cm^{-1} can be attributed to the so-called G band of carbon [35]. While the broad band at ~1320 cm^{-1} may originate from the D band of carbon and/or the two-magnon scattering of Fe$_2$O$_3$ [33,35]. The formation of carbon can be ascribed to the carbonization of oxalate in H$_2$ atmosphere [36]. Fig. 1d displays the XPS C 1s spectrum of the annealed film. The deconvolution and curve fitting of the C 1s spectrum are performed by XPSPEAK software. The C 1s peaks at 284.6, 286.7 and 288.6 eV are attributed to graphitic carbon, C−O and C=O species from surface functional groups, respectively [37]. It is noted that the peak intensity of graphitic carbon is much higher than those for C−O and C=O species. This means that the carbon element in the annealed film predominantly exists as graphitic carbon. The content of carbon in the annealed film is determined to be 5.8wt% by means of organic element analysis. The above results show that the annealed film consists of Fe$_2$O$_3$, Fe$_3$O$_4$ and carbon. In the following